Geoscience Frontiers 10 (2019) 671–682

HOSTED BY

Contents lists available at ScienceDirect

China University of Geosciences (Beijing)

Geoscience Frontiers

journal homepage: www.elsevier.com/locate/gsf

Research Paper

Advanced reliability analysis of slopes in spatially variable soils using multivariate adaptive regression splines

Leilei Liu [a], Shaohe Zhang [b,c], Yung-Ming Cheng [a,d,*], Li Liang [d]

[a] Department of Civil and Environmental Engineering, The Hong Kong Polytechnic University, Hung Hom, Kowloon, Hong Kong SAR, China
[b] Key Laboratory of Metallogenic Prediction of Nonferrous Metals and Geological Environment Monitoring, Central South University, Ministry of Education, 932 Lushan South Road, Changsha 410083, China
[c] School of Geosciences and Info-Physics, Central South University, 932 Lushan South Road, Changsha 410083, China
[d] School of Civil Engineering, Qingdao University of Technology, China

ARTICLE INFO

Article history:
Received 20 September 2017
Received in revised form
29 January 2018
Accepted 28 March 2018
Available online 9 May 2018
Handling Editor: E. Shaji

Keywords:
Slope stability
Efficient reliability analysis
Spatial variability
Random field
Multivariate adaptive regression splines
Monte Carlo simulation

ABSTRACT

This study aims to extend the multivariate adaptive regression splines (MARS)–Monte Carlo simulation (MCS) method for reliability analysis of slopes in spatially variable soils. This approach is used to explore the influences of the multiscale spatial variability of soil properties on the probability of failure (P_f) of the slopes. In the proposed approach, the relationship between the factor of safety and the soil strength parameters characterized with spatial variability is approximated by the MARS, with the aid of Karhunen–Loève expansion. MCS is subsequently performed on the established MARS model to evaluate P_f. Finally, a nominally homogeneous cohesive–frictional slope and a heterogeneous cohesive slope, which are both characterized with different spatial variabilities, are utilized to illustrate the proposed approach. Results showed that the proposed approach can estimate the P_f of the slopes efficiently in spatially variable soils with sufficient accuracy. Moreover, the approach is relatively robust to the influence of different statistics of soil properties, thereby making it an effective and practical tool for addressing slope reliability problems concerning time-consuming deterministic stability models with low levels of P_f. Furthermore, disregarding the multiscale spatial variability of soil properties can overestimate or underestimate the P_f. Although the difference is small in general, the multiscale spatial variability of the soil properties must still be considered in the reliability analysis of heterogeneous slopes, especially for those highly related to cost effective and accurate designs.

1. Introduction

Soil properties are often spatially variable (Phoon and Kulhawy, 1999; Dasaka and Zhang, 2012; Ching and Wang, 2016; Wang et al., 2016), mainly due to that soils are generally subject to complex geological, environmental, and physicochemical processes during their formation (Cho, 2012; Li et al., 2017). Such inherent spatial variability in soil properties can significantly influence the reliability analysis of slope stability. For example, a previous study (Griffiths and Fenton, 2004) noted that ignoring the spatial variability of soil properties (i.e., considering soil properties as ideally correlated materials) can overestimate the probability of failure (P_f) of a slope when the coefficients of variation (COVs) of the shear strength parameters are relatively high, or the factor of safety (FS) is relatively low. Thus, researchers have exerted increasing effort to investigate the reliability of slopes in spatially variable soils in recent years (e.g., Cho, 2010; Srivastava et al., 2010; Griffiths et al., 2011; Santoso et al., 2011; Wang et al., 2011; Ji and Low, 2012; Ji et al., 2012, 2018; Huang et al., 2013; Ji, 2014; Jiang et al., 2014, 2015; Low, 2014; Li et al., 2015; Liu et al., 2017b) to develop new reliability analysis approaches or enhance the existing approaches. Despite its approximate estimation of P_f, response surface method (RSM) has long been demonstrated as one of the most effective and efficient approaches (Jiang et al., 2014, 2015; Li et al., 2015; Jiang and Huang, 2016). However, commonly used RSMs, such as the quadratic RSM and stochastic RSM, are parametric regression methods that must be used with a prior assumption on the order and type of polynomials. Liu and Cheng (2016) demonstrated that this assumption will be misleading if the true performance function of the slope stability is a multimodal function with several peaks and troughs.

* Corresponding author.
E-mail address: ceymchen@polyu.edu.hk (Y.-M. Cheng).
Peer-review under responsibility of China University of Geosciences (Beijing).

https://doi.org/10.1016/j.gsf.2018.03.013

To maximize the efficiency of RSM and overcome the disadvantages of the traditional RSMs, this paper proposes the use of multivariate adaptive regression splines (MARS) as an efficient reliability approach for slope stability analysis in spatially variable soils. In this approach, MARS is used as a surrogate for the implicit performance function to improve the computational efficiency of FS determination. MARS is selected because of its advantage of automatically lending itself to available data samples without a prior assumption (Zhang and Goh, 2013; Liu and Cheng, 2016). MARS also displays good performance in slope reliability analysis considering single random variables in our previous work (Liu and Cheng, 2016). Nevertheless, the MARS adopted by Liu and Cheng (2016) is only suitable for spatially constant random soils; this approach cannot consider the soil spatial variability because of its inefficiency toward considerably high-dimensional problems. Hence, the proposed approach can be considered as an extension of our previous MARS model for the reliability analysis of slopes in spatially variable soils.

In addition, existing studies on slope reliability analysis in spatially variable soils present two fundamental limitations as follows: (1) the spatial variability of soil properties is simulated by stationary random fields in most of recent studies (e.g., Griffiths and Fenton, 2004; Cho, 2010; Wang et al., 2011; Jiang et al., 2014, 2015; Li et al., 2015); (2) although soil properties are assumed as non-stationary in several studies, the statistics of soil properties, such as the scale of fluctuations (SOFs), are considered the same for different soil layers (e.g., Li et al., 2015, 2016a; Jiang and Huang, 2016). Nonetheless, in geotechnical engineering practice, soil profiles are generally spatially variable on various scales (Lu and Zhang, 2007; Cho, 2012). Soil properties in different soil layers may also exhibit different SOFs (Phoon and Kulhawy, 1999; Li et al., 2015). Therefore, the influence of multiscale variability of soil properties on the reliability of heterogeneous slopes must be investigated. The present study is completed by using the proposed MARS approach due to its high efficiency. To the best of our knowledge, such study appears to be original.

This study starts with random field simulation of the inherent spatial variations of soil properties and subsequent introduction of the proposed MARS-based MCS (MARS-MCS) approach and its implementation procedure. Afterward, the MARS-MCS is illustrated through two hypothetical slope examples: (1) a statistically homogeneous slope to verify the feasibility and accuracy of MARS-MCS and (2) a two-layered cohesive slope to investigate the influence of multiscale variability of soil properties on the P_f using the proposed approach.

2. Random field simulation of spatially variable soil properties

2.1. Spatial variability of soil properties

Generally, soil properties at a particular location are closer to adjacent locations than those at far locations (Li et al., 2015). In addition, soil parameters at two arbitrary points can be hardly correlated if the absolute distance between the two points exceeds the SOF; otherwise, they are significantly correlated (Li et al., 2017). This phenomenon is the spatial variation of soil properties, which is generally characterized with an autocorrelation coefficient between soil properties at two points. Such a coefficient is commonly evaluated from an autocorrelation function (ACF), which governs the spatial correlation structure of soil properties. In geotechnical engineering practice, the real ACF for a soil is commonly difficult to obtain due to the limited site investigation data. Instead, theoretical ACFs, such as single and squared exponentials, are often used as alternatives (Li and Lumb, 1987; Li et al., 2015; Jiang and Huang, 2016; Liu et al., 2017b). Given that different ACFs yield insignificant differences in the results, and the squared exponential ACF is considerably smooth and differentiable near the origin (Li et al., 2015), this function is utilized in the present study and expressed as

$$\rho[(x_1,y_1),(x_2,y_2)] = \exp\left\{-\pi\left[\left(\frac{x_1-x_2}{\delta_h}\right)^2+\left(\frac{y_1-y_2}{\delta_v}\right)^2\right]\right\} \tag{1}$$

where (x_1,y_1) and (x_2,y_2) are the coordinates of two points in a 2-D domain; and δ_h and δ_v are the horizontal and vertical SOFs of soil properties, respectively.

2.2. Karhunen–Loève (K–L) expansion

The spatial variability of soil properties can be well modeled within the framework of random field theory. Hence, several methods such as the covariance matrix decomposition method (Wang et al., 2011), local average subdivision method (Fenton and Vanmarcke, 1990; Griffiths and Fenton, 2004) and series expansion method (Phoon et al., 2002; Sudret and Kiureghian, 2002; Cho, 2010; Jiang et al., 2014), are commonly used in the literature. A series expansion method named K–L expansion is adopted in the present study due to the following advantages (Jiang, 2014): (1) the number of discretized random variables for the desired accuracy is relatively small, thereby enhancing the random field simulation efficiency; (2) the simulated random field can be represented by a continuous function, which can be easily used to evaluate the random field property at any point in the studied domain; and (3) this expansion method can be easily extended for non-stationary random field simulations. This method is briefly described in the following.

In the context of K–L expansion, a 2-D normally distributed random field $H(x,y)$ can be discretized based on the spectral decomposition of its ACF $\rho[(x_1,y_1),(x_2,y_2)]$. This field is generally expressed as a truncated series as

$$H(x,y)\approx\widehat{H}(x,y;\theta) = \mu' + \sum_{j=1}^{M'}\sigma'\sqrt{\lambda_j}f_j(x,y)\chi_j(\theta) \tag{2}$$

where $\widehat{H}(x,y;\theta)$ is the simulated random field of $H(x,y)$; θ is the coordinate in the decomposited outcome space; μ' and σ' are the mean and standard deviation of the 2-D random field, respectively; $f_j(x,y)$ and λ_j are the eigen functions and eigen values of the 2-D ACF $\rho[(x_1,y_1),(x_2,y_2)]$ obtained by solving the homogeneous Fredholm integral equation of the second kind (Phoon et al., 2002; Jiang et al., 2015), respectively; $\chi_j(\theta)$ is a set of uncorrelated random variables with zero mean and unit variance; and M' is the number of K–L expansion terms that is critical to the accuracy and efficiency of the truncated series. Huang et al. (2001) and Laloy et al. (2013) suggested that the ratio of the expected energy (ε) can be used to measure the accuracy of the truncated series and defined ε as

$$\varepsilon = \frac{\int_{\Omega} E\left(\widehat{H}(x,\theta)-\mu\right)^2 \mathrm{d}x\mathrm{d}y}{\int_{\Omega} E(H(x,\theta)-\mu)^2 \mathrm{d}x\mathrm{d}y} = \sum_{i=1}^{M}\lambda_i \Big/ \sum_{i=1}^{\infty}\lambda_i \tag{3}$$

where $E(\cdot)$ is the expectation function, and eigen values λ_i are sorted in a descending order. Generally, a large ε value corresponds to the high accuracy of the truncated series. Moreover, ε should be close to 1 to maintain a certain accuracy. However, a large ε value also indicates a significant computation cost. To achieve a

compromise between accuracy and efficiency, Huang et al. (2001) and Laloy et al. (2013) suggested using $\varepsilon \geq 95\%$ as a criterion in determining the M value. This criterion is also used in this study.

2.3. Simulation of cross-correlated non-Gaussian random fields

In geotechnical engineering practice, a geotechnical structure is often influenced by more than one soil parameter, and different parameters are commonly cross-correlated with each other (Low, 2007; Cho, 2010; Li et al., 2011; Jiang et al., 2014). For example, the cohesion (c) and the friction angle (φ) are two key parameters that influence slope stability; these parameters are generally negatively correlated (Cho, 2010). Evidently, all these parameters should be simulated as cross-correlated random fields when the spatial variability of soil properties is considered. According to Cho (2010), all random fields simulated over the same region Ω (e.g., a soil layer) share an identical ACF; the cross-correlation structure between each pair of simulated fields can be defined by a cross-correlation coefficient. The underlying rationale of this statement lies in that the spatial correlation structure is generally caused by changes in the constitutive nature of the soil over space (Fenton and Griffiths, 2003; Cho, 2010). Therefore, only one evaluation of the eigen modes of a given ACF is required for a pair of cross-correlated random fields over a region Ω. The resultant set of eigen functions and eigen values is subsequently used in combination with two cross-correlated sets of random variables to expand the cross-correlated random fields. In the following, the simulations of cross-correlated random fields associated with c and φ are used as examples to illustrate the procedure for cross-correlated random field simulations (Cho, 2010; Jiang et al., 2014).

If the eigen modes and the number of the K–L expansion terms under a given ACF (e.g., squared exponential ACF in this study) are known, the cross-correlated random fields between c and φ can be simulated only if the cross-correlated sets of random variables are obtained. When the cross-correlation coefficient between c and φ as $\rho_{c\varphi}$ is denoted, the cross-correlation matrix between them can be written as

$$R = \begin{bmatrix} 1 & \rho_{c\varphi} \\ \rho_{c\varphi} & 1 \end{bmatrix} \tag{4}$$

A vector of independent standard normal samples is subsequently generated using Latin hypercube sampling (LHS) or a standard normal generator. This vector is finally partitioned into N_F vectors with a dimension of M' to form a sample matrix $(\chi)_{M' \times N_F}$, where N_F is the number of random fields to be simulated. For two random fields simulated here, $N_F = 2$ and $\boldsymbol{\chi} = \{\boldsymbol{\chi}_c \quad \boldsymbol{\chi}_\varphi\}$, where $\boldsymbol{\chi}_c = \{\chi_{c1} \quad \chi_{c2} \quad \cdots \quad \chi_{cM'}\}^T$ and $\boldsymbol{\chi}_\varphi = \{\chi_{\varphi 1} \quad \chi_{\varphi 2} \quad \cdots \quad \chi_{\varphi M'}\}^T$. Afterward, a lower triangular matrix L is obtained by the Cholesky decomposition of R. According to χ and L, the cross-correlated standard normal sample matrix ξ is obtained as

$$\xi = \chi L^T = \{\xi_c \quad \xi_\varphi\} \tag{5}$$

where $\xi_c = \{\xi_{c1} \quad \xi_{c2} \quad \cdots \quad \xi_{cM'}\}^T$ and $\xi_\varphi = \{\xi_{\varphi 1} \quad \xi_{\varphi 2} \quad \cdots \quad \xi_{\varphi M'}\}^T$.

Given that the eigen modes and the cross-correlated standard normal sample matrix ξ are known, the cross-correlated Gaussian random fields underlying c and φ are discretized as

$$\widehat{H}_i^G(x,y) = \mu_i + \sum_{j=1}^{M'} \sigma_i \sqrt{\lambda_j} f_j(x,y) \xi_{ij} \quad (for\ i = c, \varphi) \tag{6}$$

The isoprobability transformation (Li et al., 2011) is then utilized to obtain the cross-correlated non-Gaussian random fields component-to-component as

$$\widehat{H}_i^{NG}(x,y) = G_i^{-1}\left\{\Phi_i\left[\widehat{H}_i^G(x,y)\right]\right\} \quad (for\ i = c, \varphi) \tag{7}$$

where $G_i^{-1}(\cdot)$ is the inverse cumulative distribution function (CDF) of each non-Gaussian random field $H_i^{NG}(x,y)$, and $\Phi_i(\cdot)$ is the CDF of each Gaussian random field $H_i^G(x,y)$. For example, if c and φ are assumed as cross-correlated lognormal random fields, then the lognormal fields can be easily approximated by exponentiating their approximate Gaussian random fields as

$$\widehat{H}_i^{LNG}(x,y) = \exp\left[\mu_{\ln i} + \sum_{j=1}^{M'} \sigma_{\ln i} \sqrt{\lambda_j} f_j(x,y) \xi_{ij}\right] \quad (for\ i = c, \varphi) \tag{8}$$

where $\mu_{\ln i}$ and $\sigma_{\ln i}$ are the mean and standard deviation of the Gaussian random field $\ln i$, respectively. The relationship between (μ_i, σ_i) and $(\mu_{\ln i}, \sigma_{\ln i})$ is given as

$$\begin{cases} \mu_{\ln i} = \ln \mu_i - 0.5\sigma_{\ln i}^2 \\ \sigma_{\ln i} = \sqrt{\ln\left[1 + (\sigma_i/\mu_i)^2\right]} \end{cases} \tag{9}$$

3. MARS-MCS for slope reliability analysis

Typically, the limit state function (LSF) of a slope is highly nonlinear, and direct evaluation of the FS values on a deterministic stability model within the framework of MCS is very time-consuming. In this section, an MARS-based RSM is proposed to serve as an approximate surrogate for the true LSF of the slope, based on which the slope reliability analysis can be efficiently performed.

3.1. Introduction of MARS

MARS was initially proposed by Friedman (1991), which provides a flexible statistical tool to approximate the relationship between a set of independent variables and their responses. According to MARS, the true function $f(X)$ can be approximated as

$$f(X) \approx \widehat{f}(X) = a_0 + \sum_{m=1}^{M} a_m B_m(X) \tag{10}$$

where $\widehat{f}(X)$ is the MARS predictor; $X = (x_1, x_2, \cdots, x_p)$ is a vector of input variables; a_m is the coefficient of the mth term in Eq. (10) obtained by the least squares method; and $B_m(X)$ is the mth basis function (BF) or spline consisting of a product of several $b_{km}(\cdot)$, which is written as

$$B_m(X) = \prod_{k=1}^{K_m} b_{km}\left(x_{v(k,m)} | p_{k,m}\right) \tag{11}$$

where K_m is the number of $b_{km}(\cdot)$, which is a two-sided truncated power function that is referred to as the spline basis function (SBF) in the form of

$$\begin{aligned} b_{km}\left(x_{v(k,m)} \middle| p_{k,m}\right) &= \left[s_{k,m} \times \left(x_{v(k,m)} - t_{k,m}\right)\right]_+^q \\ &= \max\left(0, s_{k,m} \times \left(x_{v(k,m)} - t_{k,m}\right)^q\right) \end{aligned} \tag{12}$$

where $s_{k,m}$ is the truncation direction with the value $+1$ or -1;

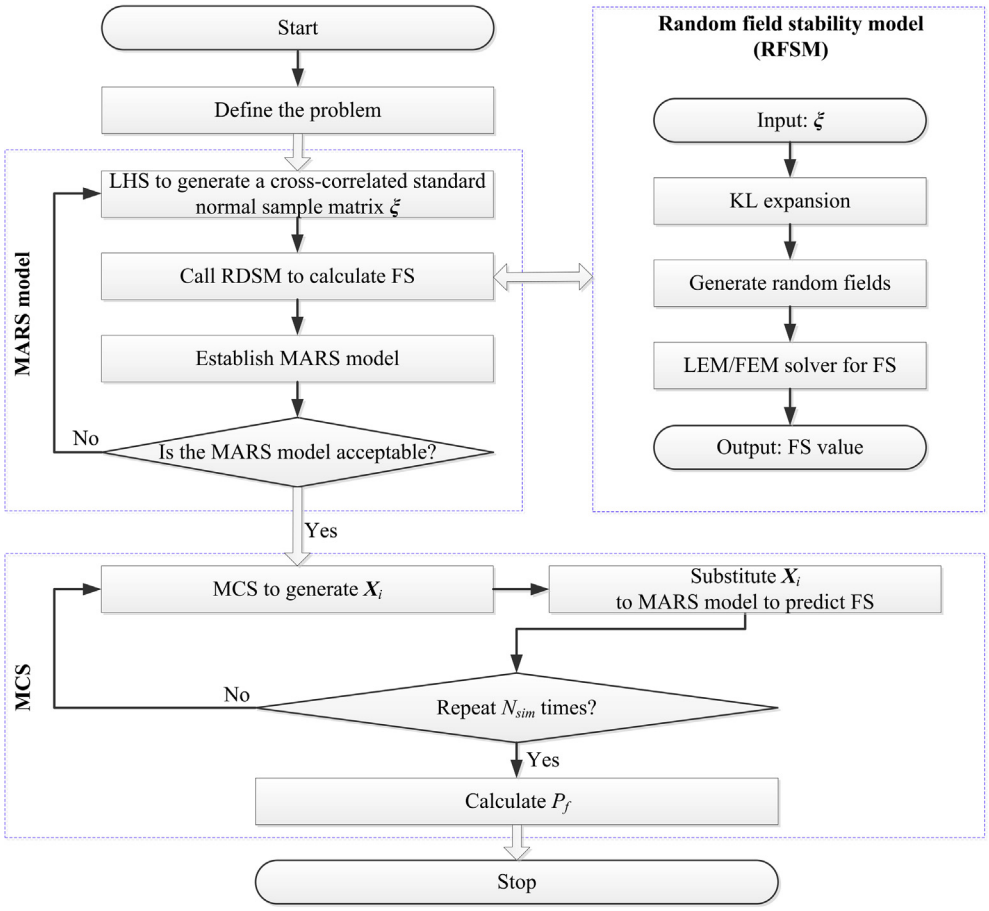

Figure 1. Flow chart for MARS–MCS.

$x_{v(k,m)}$ is the input variable that corresponds to the kth truncated SBF in the mth term of Eq. (10); $t_{k,m}$ is the knot that marks the end of an interval and the beginning of another interval with respect to the input variable $x_{v(k,m)}$; and q is a non-negative parameter that is the power of SBF reflecting a different degree of smoothness of the resulting MARS estimation. To simplify the process, only piecewise cubic ($q = 3$) function is examined in this study. Note that $B_m(X)$ can be a single SBF as well as the product of two or more SBFs.

Regarding the implementation of MARS, it is achieved by a two-phase process: forward selection and backward pruning. The forward phase starts with only the basis function $B_0(X) = 1$ in the MARS model, followed by the identification of the paired BFs that yield the largest decrease in training error when they are added to the current model. Assume a current model with M BFs and after two BFs are added, the next model would be updated as

$$\widehat{f}(X) = a_0 + \sum_{m=1}^{M} a_m B_m(X) + \widehat{a}_{m+1} B_l(X)\max(0, x_j - t) + \widehat{a}_{m+2} B_l(X)\max(0, t - x_j) \quad (13)$$

where $\widehat{a}_{m+1}$ and $\widehat{a}_{m+2}$ are estimated by the least squares method and $B_l(X)$ is the formerly determined BF with $0 \le l \le M$. This forward process of adding BFs continues until the predefined maximum number of terms or the threshold of the training error is reached. Generally, this process will produce a very complex and over-fitted model which may poorly predict other new points; however it well fits the training data sets (e.g., Cheng and Cao, 2014).

To enhance the predictive ability of the MARS model, the backward pruning phase is then employed to delete the redundant BFs that have the smallest contribution to the model. At each step, the least effective BF in the current model will be deleted, which produces a submodel with one BF less than the current model. This process is repeated until no BF is available to be deleted, with which a group of submodels is generated. Then, the best MARS model is identified as the submodel that has the lowest value of GCV (generalized cross-validation). For a training data set with N points, GCV is calculated as (e.g., Hastie et al., 2009)

$$GCV = \frac{\frac{1}{N}\sum_{i=1}^{N}\left[y_i - \widehat{f}(X_i)\right]^2}{\left[1 - \frac{M + d \times (M-1)/2}{N}\right]^2} \quad (14)$$

where y_i is the true value at X_i; $\widehat{f}(X_i)$ is the predictive value at X_i; d is a penalizing factor with a default value of 3 according to Friedman (1991).

3.2. Evaluation of P_f using MARS–MCS

Having established the RSM of a slope stability using MARS, the FS for any given vector of random variables $X = (x_1, x_2, \cdots, x_p)$ can be easily calculated, where p is the number of the random variables. It should be noted that each vector of random variables here comes from a realization of the discretizations of the random fields underlying the soil properties. For example, for a slope involving two

cross-correlated random fields, according to the above analysis in Section 2.3, the two random fields can be discretized by two cross-correlated vectors of random variables, and each of the vectors has the same sample size (e.g., M'). In this case, the total number of the discretized random variables is equal to $2M'$, i.e., $p = 2M'$. An MCS with a total number of N_{sim} realizations of random fields is then directly performed on the established MARS to evaluate the P_f as

$$P_f = \frac{1}{N_{sim}} \sum_{i=1}^{N_{sim}} I\{FS[X_i] < 1\} \tag{15}$$

where $I\{\cdot\}$ is an indicator function that is equal to unity when $FS[X_i]\langle 1$ and zero otherwise; and $FS[X_i]$ is the FS for a given X_i. Since $FS[X_i]$ is directly calculated from the MARS model instead of the initially established deterministic slope stability model, so the proposed MARS-based MCS is more computationally efficient.

4. Implementation procedure of MARS–MCS

To facilitate the understanding and application of the MARS–MCS approach, this section introduces the detailed procedure for implementing the proposed approach in practice. For convenient purpose, the procedure is schematically shown in Fig. 1, which comprises three major modules: random field stability model (RFSM) for the direct FS evaluation of a spatially varied slope using a limit equilibrium method/finite element method (LEM/FEM), MARS model to construct the approximate surrogate for the true LSF of a slope, and MCS for calculating the P_f. Afterward, the probabilistic analysis of a 2-D slope involving two cross-correlated random fields is used as an example to elaborate the whole procedure step by step as follows:

(1) *Model preparation*. Characterize the slope geometry and collect all the soil parameters required for both deterministic and probabilistic slope stability analysis, such as the means, standard deviations, cross-correlation coefficients, probability distributions, SOFs, and ACFs.

(2) *Construct the RFSM*. The main purpose of this step is to equip the conventional LEM/FEM with the ability to calculate the FS of a slope in spatially variable soils. This requires one to characterize the spatial variability of soil properties by random fields, and then to incorporate them into an LEM/FEM model. Details are given as follows:
   (a) Solve the 2-D homogeneous Fredholm integral equation using the suggested method in section 2.2 to obtain the eigen functions $f_j(\cdot)$ and eigen values λ_j of the selected ACF in step (1). Then, determine the number (i.e., M') of K–L expansion terms based on the ratio of the expected energy ε in Eq. (3).
   (b) Discretize the study domain into finite elements and extract the centroid coordinates (x_i, y_i) of each element. Then, given a cross-correlated standard normal sample matrix sample matrix ξ, the cross-correlated non-Gaussian random fields can be easily obtained by using Eqs. (6)–(9). The soil properties at different locations (x_i, y_i) are then calculated by substituting their coordinates into Eq. (11), which is considered as one realization of the random fields.
   (c) Assign the soil properties at different locations (x_i, y_i) to their corresponding random field elements in an LEM/FEM model to calculate the FS value.

(3) *MARS model calibration and validation*. Like many other RSM, a certain number of training data are first required to calibrate the MARS model. In this study, these training data are obtained as follows:
   (a) Use LHS to generate a vector of standard normal samples, which are then partitioned into N_F columns (e.g., two herein) with a dimension of M' to form an uncorrelated standard normal sample matrix $(\chi)_{M' \times N_F}$.
   (b) Transform the χ to a cross-correlated standard normal sample matrix ξ using Eq. (5), which is then substituted into RDSM to obtain the FS.
   (c) The above procedure is repeated for N_t times until N_t pairs of training data (χ, FS) are obtained. These data are then used to calibrate the MARS model.
   (d) Validate the established MARS model by a small group of testing data that can be obtained using the suggested procedure in steps (a) and (b). If the accuracy of the model is not good, then go back to step (a) to increase the number of the training data until the accuracy is acceptable.

(4) *MCS for calculating the P_f*. Randomly generate N_{sim} vectors of standard normal samples $(X)_{N_F \cdot M' \times N_{sim}}$, which are subsequently substituted into the established MARS model to obtain the predictive values of FS. The P_f is thus easily obtained based on Eq. (15).

5. Example I: Application to a c–φ slope

This section investigates the reliability of a statistically homogeneous c–φ slope using the proposed approach. The slope was also analyzed by in the literature (Cho, 2010; Li et al., 2015; Liu et al., 2017b). Thus, the results obtained from previous studies can be used directly to validate the accuracy of the proposed approach.

5.1. Example description and deterministic analysis results

Fig. 2 shows the geometry of the slope, which comprises a "homogeneous" soil layer with a height of 10 m and a slope angle of 45°. The soil parameters for the probabilistic stability analysis are summarized in Table 1. The unit weight of the soil is considered constant with a value of 20 kN/m^3. The c and φ are simulated as cross-correlated lognormal random fields with a cross-correlation coefficient of −0.5. The mean and COV of the random field underlying the c are respectively 10 kPa and 0.3; correspondingly, the counterparts of the φ are 30° and 0.2, respectively. According to these mean values, the deterministic slope stability model is initially established using the Bishop's simplified method (BSM), which yields an FS of 1.205 with the critical slip surface passing through the slope toe, as shown in Fig. 2. Furthermore, the FS value is highly similar to those obtained by Cho (2010) and Li et al. (2015) by using the same method, i.e., 1.204 and 1.208, respectively, which indicates the correctness of the model.

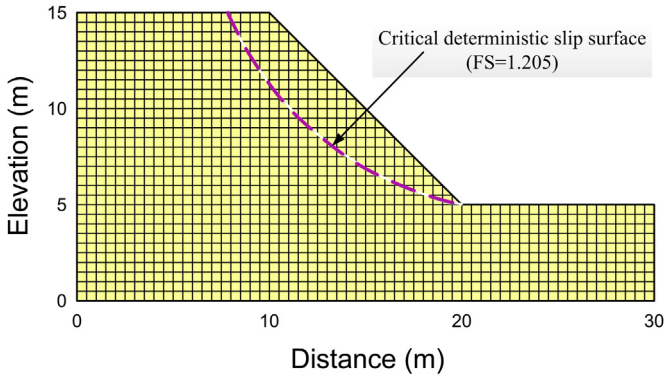

Figure 2. Geometry and random field discretization of the c–φ slope.

Table 1
Statistics of soil parameters for Example I.

Parameter	Mean	COV	Distribution	SOF	$\rho_{c\varphi}$
c	10 kPa	0.3	Lognormal	$\delta_h = 40$ m, $\delta_v = 4$ m	−0.5
φ	30°	0.2	Lognormal	$\delta_h = 40$ m, $\delta_v = 4$ m	
γ	20 kN/m^3	–	–	–	–

Note: The symbol "–" means not applicable.

Fig. 2 also illustrates the random field discretization of the slope domain, which consists of 1190 four-noded quadrilateral elements and 20 three-noded triangular elements. This random field mesh is based on that used by Li et al. (2015) and Liu et al. (2017b) to achieve a consistent comparison with their results in the following analysis. The random fields are subsequently discretized at the centroid coordinates of each random field element to characterize the spatial variability of soil parameters by using the suggested method in Section 2 (Li et al., 2015; Liu et al., 2017b) and the assumed SOFs listed in Table 1, i.e., $\delta_h = 40$ m and $\delta_v = 4$ m. Herein, the effect of the size of the random field element is not considered. Further details on the selection of the random field element size are provided elsewhere (Ching and Phoon, 2013). In the following, probabilistic slope stability analysis is conducted using the proposed approach with the aforementioned soil parameters.

5.2. Probabilistic analysis results

The MARS model is first established on the basis of a certain number of training samples, which are generated by LHS prior to being applied to evaluate the P_f of the c–φ slope. The number of the training samples is crucial to the accuracy of the MARS model. A large number of samples can increase the model accuracy and decrease the simulation efficiency. The balance between computational accuracy and efficiency must be maintained. Nonetheless, no precise guidelines have been established regarding this issue in the literature (Kang et al., 2015). Hence, in the present study, an empirical guideline that 10D–15D (D is the number of variables) samples will exert no remarkable change on the model performance is adopted in accordance with the works of Silvestrini et al. (2013). Kang et al. (2015) demonstrated that this guideline is useful. The case in Table 1 is used as an example to illustrate the performance of the guideline. When $\delta_h = 40$ m and $\delta_v = 4$ m, for the squared exponential ACF, the number of K–L expansion terms to be maintained in Eq. (4) is 14 according to Fig. 3; this number is based on the criterion shown in Eq. (5). The total number of random variables is 28 because two cross-correlated random fields are considered herein. Consequently, according to the guideline, 280 LHS samples are first generated to calibrate the MARS model. Results shown in Fig. 4 illustrated that the MARS model fits the 280 sample data considerably well with a R^2 of approximately 0.9934. This model also shows a relatively high predictive ability when evaluated by a set of 100 randomly generated samples. This finding demonstrated the feasibility of the guideline. Notably, the sample size should be increased if the 10D training samples cannot yield an accurately calibrated model, which will consume many computational resources. This adjustment is the same as that utilized by Kang et al. (2015), which, unless otherwise specified, is also adopted in the following analysis of this study.

No rules have been established on how to increase the size of the training data, except for a trial and error method. Moreover, in some cases, a surrogate model calibrated by 15D training samples cannot yield satisfactory results because the slope stability problem is highly complex. This phenomenon may become remarkably serious when the number of discretized random variables is relatively small, as demonstrated by Ji et al. (2017). In view of these problems, a comprehensive empirical guideline proposed by Ji et al. (2017) may be useful. This guideline is given as follows: if the number of the discretized random variables is relatively small (e.g., less than 10), then the surrogate model should be trained based on 100–200 training data generated by a specially treated LHS

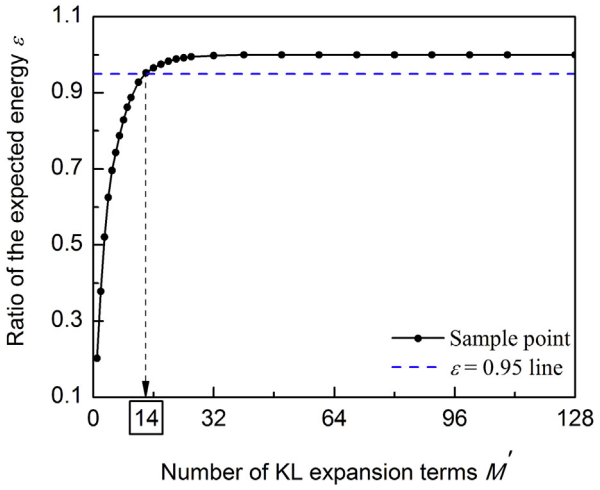

Figure 3. Variation of the ratio of the expected energy ε with the number of K–L expansion terms for the case in Table 1.

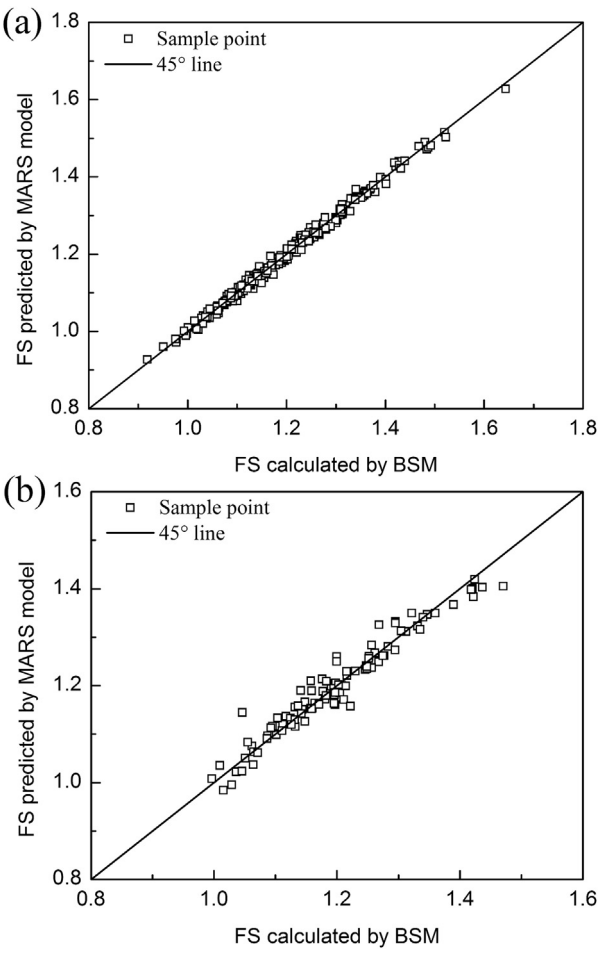

Figure 4. Validation of MARS model for the case in Table 1. (a) 280 training samples, $R^2 = 0.9934$; (b) 100 testing samples, $R^2 = 0.9423$.

Table 2
Reliability results obtained by different methods for different cases in Example I.

Methods	δ_h (m)	δ_v (m)	μ_{FS}	σ_{FS}	COV_{FS}	P_f
MARS–MCS (this study)	40	4	1.198	0.114	0.096	2.92×10^{-2}
10,000 LHS (this study)			1.198	0.116	0.096	2.72×10^{-2}
10,000 LHS [47]			1.184	0.103	0.087	2.21×10^{-2}
Multiple RSM [15]			1.195	0.102	0.085	1.87×10^{-2}
50,000 MCS [14]			1.199	0.106	0.088	1.71×10^{-2}
Subset simulation [19]			1.197	0.103	0.086	2.04×10^{-2}
MARS–MCS (this study)	40	8	1.201	0.140	0.117	5.46×10^{-2}
10,000 LHS (this study)			1.200	0.142	0.118	5.70×10^{-2}
10,000 LHS [47]			1.189	0.123	0.103	4.15×10^{-2}
Multiple RSM [15]			1.195	0.119	0.100	3.97×10^{-2}
50,000 MCS [14]			1.202	0.126	0.105	3.70×10^{-2}
Subset simulation [19]			1.199	0.126	0.105	4.10×10^{-2}
MARS–MCS (this study)	80	4	1.201	0.117	0.097	3.05×10^{-2}
10,000 LHS (this study)			1.198	0.117	0.098	2.86×10^{-2}
10,000 LHS [47]			1.185	0.105	0.089	2.38×10^{-2}
Multiple RSM [15]			1.196	0.104	0.087	2.06×10^{-2}
50,000 MCS [14]			1.200	0.109	0.091	1.91×10^{-2}
Subset simulation [19]			1.200	0.107	0.089	2.20×10^{-2}

Note: A training sample size of 10*D* was adopted for all cases in this table.

technique; otherwise, the 10*D*−15*D* guideline for high-dimensional random variables should be used. Details on further explanations of this guideline can be found in the work of Ji et al. (2017).

Afterward, an MCS with a total of 1,000,000 samples is performed directly on the calibrated MARS model to calculate the P_f of the slope. To validate the accuracy of the proposed MARS–MSC, a direct LHS with a total of 10,000 samples based on the original deterministic stability model is also conducted. Literature results are also referred for comparison. Results from both the present study and literature, including the statistics of FS (i.e., mean μ_{FS}, standard deviation σ_{FS}, and coefficient of variation COV_{FS}) and the values of P_f for three different cases, are presented in Table 2. The P_f values (i.e., 2.92×10^{-2}, 5.46×10^{-2}, and 3.05×10^{-2}) obtained from the proposed MARS-MCS for the three cases are in good consistence with the "exact" results (i.e., 2.72×10^{-2}, 5.70×10^{-2}, and 2.86×10^{-2}) evaluated by the direct LHS of this study, respectively. Furthermore, for all the three cases considered herein, the probabilities of failure obtained by both the MARS−MCS and the direct LHS in the present study are marginally larger than those obtained by Cho (2010), Jiang (2014), Li et al. (2015) and Liu et al. (2017b). The difference is mainly due to that the squared exponential ACF and the single exponential ACF are used in this study and their studies to characterize the spatial variation of soil properties, respectively. This explanation is reasonable and validated by Li et al. (2015) who stated that: "The probability of failure associated with the commonly-used single exponential ACF may be underestimated." Nevertheless, the difference between these methods is minimal. The statistics of FS obtained by different methods for all cases are also approximately similar. Overall, these findings indicated that the proposed MARS−MCS can accurately evaluate the reliability of slopes in spatially variable soils.

5.3. Influence of the statistics of soil properties on the accuracy of MARS–MCS

This section further explores the effects of different statistics (e.g., COVs and SOFs) of soil properties on the accuracy of the proposed MARS–MCS for reliability analysis. For this purpose, the aforementioned statistics including $\rho_{c\varphi}$, COV_c, COV_φ, δ_h and δ_v are allowed to vary within some specified ranges to perform parametric studies—$\rho_{c\varphi} \in [-0.7, 0.5]$, $COV_c \in [0.1, 0.7]$, $COV_\varphi \in [0.05, 0.20]$, $\delta_h \in [10\text{ m}, 60\text{ m}]$ and $\delta_v \in [1\text{ m}, 6\text{ m}]$. These ranges are the same as those adopted by Li et al. (2015), and thus the capacity of the proposed MARS–MCS can be compared easily with the results reported by Li et al. (2015). In addition, following Li et al. (2015), only one statistical parameter is changed during each parametric study, while the other parameters are kept the same as the nominal case where $\rho_{c\varphi} = 0, COV_c = 0.3, COV_\varphi = 0.2, \delta_h = 40\text{ m}$ and $\delta_v = 4\text{ m}$.

Fig. 5 shows the variations of P_f obtained by this study and several other methods in the literature with respect to the $\rho_{c\varphi}$. In general, the results obtained by different methods show a very similar variation trend, increasing with the value of $\rho_{c\varphi}$. The difference between the failure probabilities obtained by this study and those from literature is significant at small values of the $\rho_{c\varphi}$ but minimal when cohesion and friction angle are highly positively correlated (e.g., $\rho_{c\varphi} = 0.5$). For example, when $\rho_{c\varphi} = -0.7$, the P_f is predicted as 7.2×10^{-3} using the proposed MARS−MCS, whereas the values of P_f are approximately 3.9×10^{-3}, 4.86×10^{-3} and 4.3×10^{-3} by Cho (2010), Li et al. (2015) and Liu et al. (2017b), respectively. Such difference is expected because the single exponential ACF commonly used in these literature would underestimate the failure probability, as stated before and validated by Li et al. (2015). However, the results are of the same order of magnitude, which also verifies the accuracy of the MARS−MCS to some extent. Furthermore, to ensure the results by MARS–MCS be more convincing, results from direct LHS are also plotted in Fig. 5 and are considered as the "exact" solutions here. Note that, considering the computation efficiency and the potential probability level, the sample sizes of the LHS are 1000, 1000, 5000, 5000, 10,000 and 30,000 for $\rho_{c\varphi} = [0.5, 0.25, 0, -0.25, -0.5, -0.7]$, respectively. As seen from Fig. 5, the curve of the LHS is nearly consistent with the one associated with MARS−MCS, suggesting the high accuracy of the proposed approach.

Fig. 6a and b compares the reliability results obtained by the MARS–MCS and the multiple RSM for various values of COV_c and COV_φ, respectively. The results associated with the multiple RSM are taken directly from the work by Li et al. (2015). It should be noted that, to keep a consistent comparison, only the results based on the squared exponential ACF are plotted in the figures as a reference, though the failure probabilities were also evaluated based on several other ACFs in the work by Li et al. (2015). For different values of both COV_c and COV_φ, a good agreement between the two approaches is identified from Fig. 6, indicating the high accuracy and robustness of MARS–MCS against the COVs of soil properties.

To investigate the influence of different SOFs on the capability of the MARS–MCS, Fig. 7a and b shows the variations of P_f obtained by

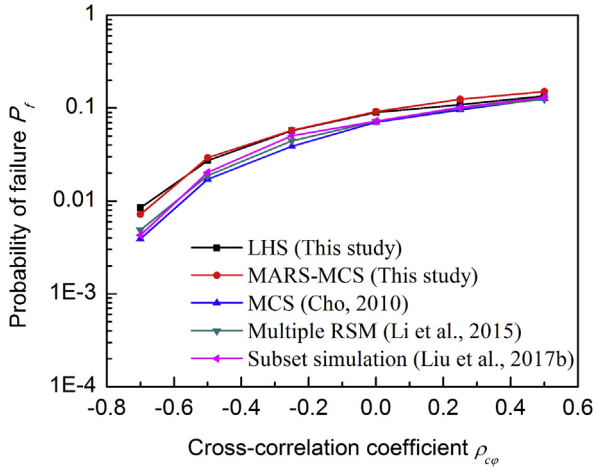

Figure 5. Comparison of reliability results obtained by different methods for various values of $\rho_{c\varphi}$ in Example I.

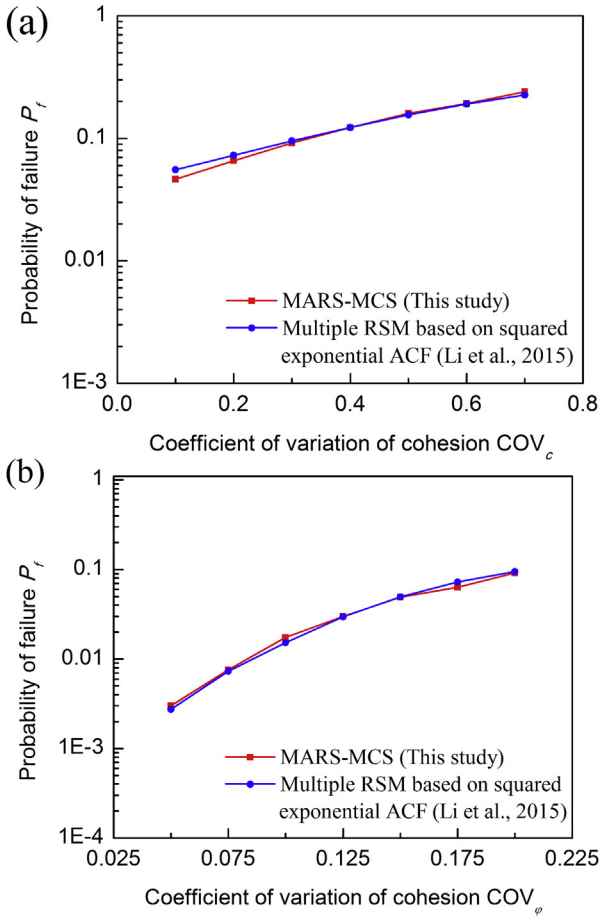

Figure 6. Comparison of reliability results obtained by different methods for various COVs in Example I. (a) Cohesion; (b) friction angle.

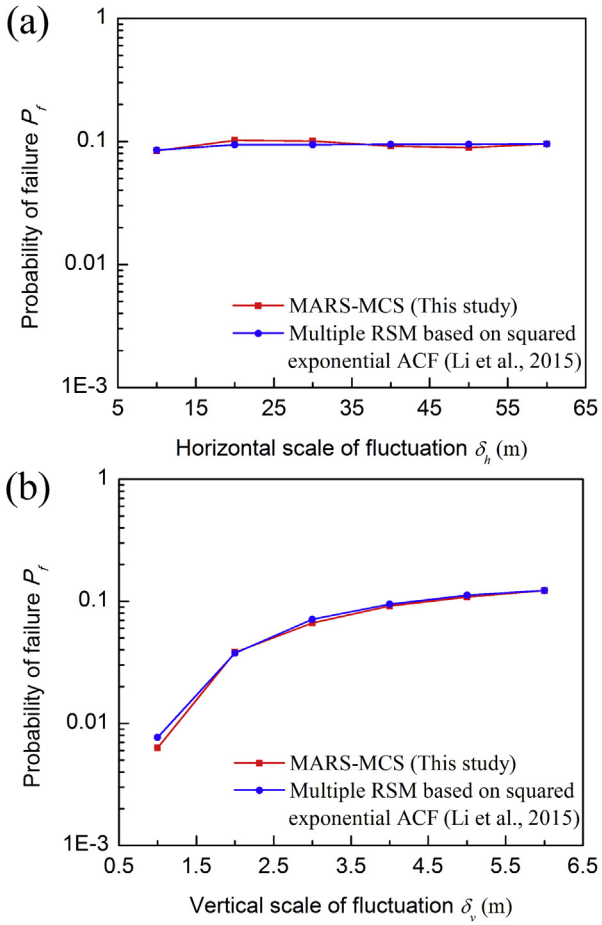

Figure 7. Comparison of reliability results obtained by different methods for various SOFs in Example I. (a) Horizontal scale of fluctuation; (b) vertical scale of fluctuation.

the MARS–MCS and the multiple RSM with respect to δ_h and δ_v, respectively. Similar to Fig. 6, the results evaluated by the MARS–MCS agree well with those obtained from the multiple RSM based on the squared exponential ACF (e.g., Li et al., 2015). For example, the P_f estimated using the proposed approach increases from 6.3×10^{-3} to 0.123 when δ_v changes from 1 m to 6 m, which is similar to the variation of the P_f obtained by the multiple RSM within the same range, from approximately 7.66×10^{-3} to 0.122. This suggests the effectiveness of the MARS–MCS for both high- and low-probability levels. Totally, it can be concluded that the MARS–MCS can accurately evaluate the reliability of slopes in differently spatially varied soils.

6. Example II: Application to a two-layered cohesive slope

Having demonstrated the capability of the proposed MARS–MCS approach for the reliability analysis of a statistically homogeneous c–φ slope under different spatially varied soil properties, this section further extends the MARS–MCS approach for the reliability analysis of a two-layered cohesive slope. Meanwhile, based on this heterogeneous slope example, the influence of the multiscale spatial variability of soil properties on slope reliability analysis is investigated using the proposed approach, which appears to be original to the best of our knowledge.

6.1. Example description and deterministic analysis results

As shown in Fig. 8, the heterogeneous slope as studied is adapted directly from the first slope example, which has the same slope height (i.e., 10 m) and slope angle (i.e., 45°) but comprises of two undrained clay layers. The soil parameters for the probabilistic stability analysis are tabulated in Table 3. As shown in the table, the unit weight of the cohesive soil layer that extends to 15 m below the top of the slope is considered constant with a value of 19 kN/m^3, whereas the undrained shear strengths of the two clay layers, s_{u1} and s_{u2}, are simulated as independent lognormal random fields. The mean and COV of the random field s_{u1} are 51 kPa and 0.3, respectively, while the counterparts of the random field s_{u2} are 34 kPa and 0.3, respectively. As a reference, based on the mean values, the deterministic stability model for the slope was initially established using BSM which gave the FS as 1.394 with the critical slip surface passing through the slope toe, as shown schematically in Fig. 8.

Fig. 8 also shows the random field discretization of the cohesive slope, which is the same as the discretization of the first slope example because the two slope examples share the same slope geometry. Based on the discretized elements, the random fields of s_{u1} and s_{u2} can be easily simulated to characterize the spatial variability of soil parameters using the same method adopted in the first example and the SOFs listed in Table 3. However, different from Example I, s_{u1} and s_{u2} here should be simulated as globally non-stationary random fields because the soil properties from different soil layers generally exhibit multiscale spatial variations due to different formation processes (e.g., Cho, 2012). This indicates that the soil properties at any two locations in different soil layers are uncorrelated. Extention of the K–L expansion for non-stationary random field simulations is straightforward. Interested readers are

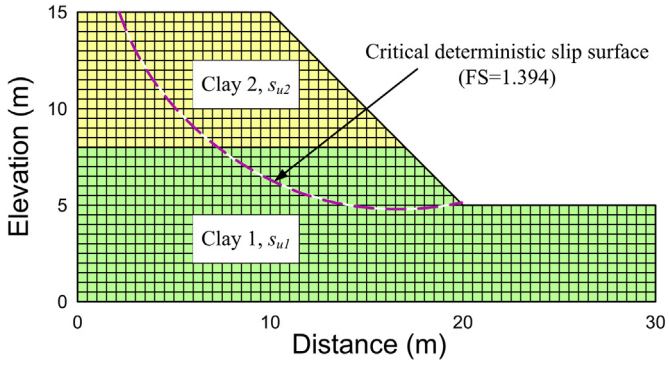

Figure 8. Geometry and random field discretization of the cohesive slope.

referred to Lu and Zhang (2007), Jiang and Huang (2016) and Liu et al. (2017a) for more details. In the following, probabilistic analysis for the cohesive slope is performed using the proposed MARS–MCS approach based on globally non-stationary random fields.

6.2. Probabilistic analysis results

To evaluate the P_f of the cohesive slope, MARS model is first established based on a certain number of training samples that are generated by LHS. The size of the training samples is determined using the strategy introduced in Section 5.2 to maintain a balance between the computational accuracy and efficiency. For illustration, the case in Table 3 is taken as an example to show the usefulness of this strategy for the heterogeneous slope. When $\delta_h = 40$ m, $\delta_v = 4$ m and the squared exponential ACF are applied to both random fields of s_{u1} and s_{u2}, the number of K–L expansion terms to be maintained in Eq. (4) is identified as 8 and 6 respectively, as shown in Fig. 9. The total number of random variables is thus calculated as 14. Based on the aforementioned strategy and from an internal study, it is found that 15D (i.e., 210) samples can well calibrate the MARS model with a good predictive ability. The results are shown in Fig. 10, and it is found from the figure that the MARS model fits the 210 sample data very well with an R^2 of about 0.9905 which is a relatively high predictive ability when the model is tested by a set of 100 randomly generated samples. Next, MCS can be well performed directly on the calibrated MARS model to evaluate the P_f of the cohesive slope.

For the case in Table 3, the P_f is calculated as 8.17×10^{-2} using the proposed MARS–MCS approach with a total of 1,000,000 MCS samples. This value of P_f is very consistent with the result (i.e., 8.25×10^{-2}) estimated by 10,000 direct LHS on the original deterministic stability model. Furthermore, four more cases with different SOFs in different soil layers are considered to further validate the accuracy of the proposed approach. Both the proposed approach and LHS are performed on these cases, and the results are tabulated in Table 4. From the table, it is observed that the values of P_f (i.e., 8.81×10^{-2}, 6.89×10^{-2}, 7.88×10^{-2} and 6.46×10^{-2}) obtained from the proposed approach for the four cases (i.e., Case No. 2 to No. 5) compare favorably with the "exact" results (i.e., 7.87×10^{-2}, 5.89×10^{-2}, 7.11×10^{-2} and 6.31×10^{-2}) that are evaluated by the direct LHS of this study, respectively. However, for the similar results, the proposed MARS–MCS only requires a limited number of calls (e.g., $15D = 210$ in case No. 1) of the time-consuming deterministic stability model, which is much more efficient than the direct LHS with 10,000 samples. In addition, the statistics of FS obtained by different methods for all cases are

Table 3
Statistics of soil parameters for Example II.

Parameter	Mean	COV	Distribution	SOF
s_{u1}	51 kPa	0.3	Lognormal	$\delta_{h1} = 40$ m, $\delta_{v1} = 4$ m
s_{u2}	34 kPa	0.3	Lognormal	$\delta_{h2} = 40$ m, $\delta_{v2} = 4$ m
γ	19 kN/m^3	–	–	–

Note: The symbol "–" means not applicable.

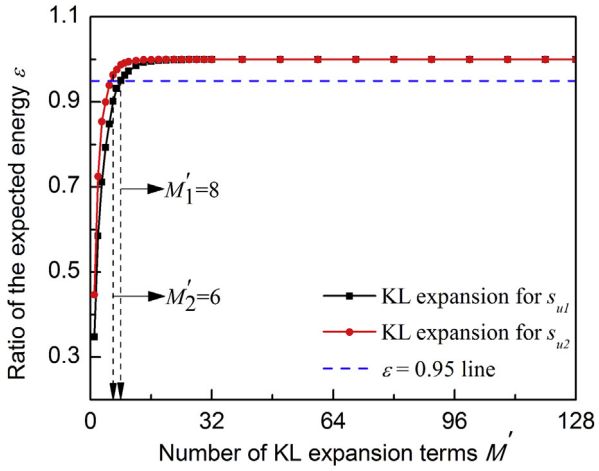

Figure 9. Variation of the ratio of the expected energy ε with the number of K–L expansion terms for the case in Table 3.

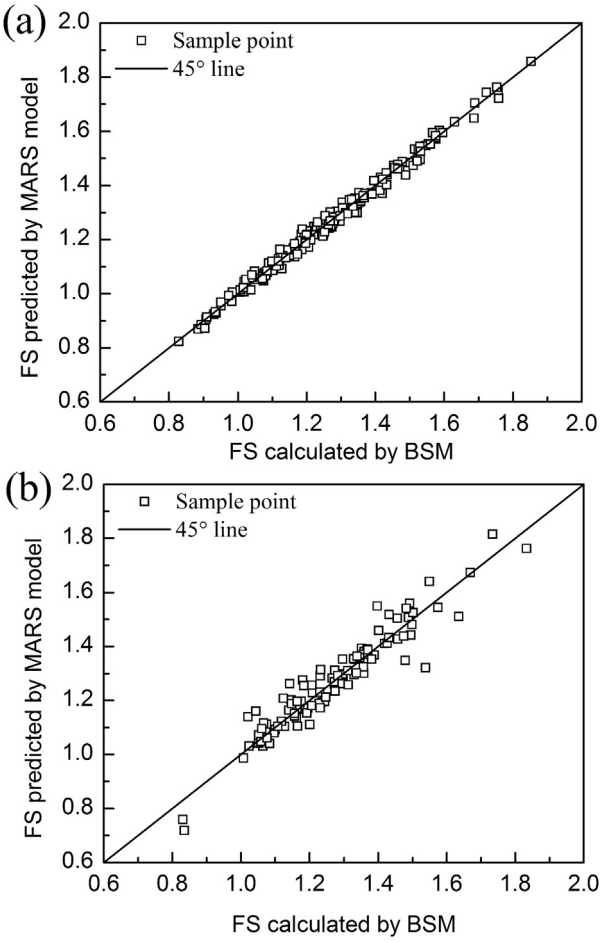

Figure 10. Validation of MARS model for the case in Table 3. (a) 210 training samples, $R^2 = 0.9905$; (b) 100 training samples, $R^2 = 0.9001$.

Table 4
Reliability results obtained by different methods for different cases in Example II.

No.	Case	Method	N_t	μ_{FS}	σ_{FS}	COV_{FS}	P_f	Relative error of P_f
1	$\delta_{h1} = 40$ m, $\delta_{v1} = 4$ m	MARS–MCS (this study)	15*D*	1.259	0.195	0.155	8.17×10^{-2}	0.010
	$\delta_{h2} = 40$ m, $\delta_{v2} = 4$ m	10,000 LHS	–	1.254	0.191	0.152	8.25×10^{-2}	
2	$\delta_{h1} = 40$ m, $\delta_{v1} = 4$ m	MARS–MCS (this study)	20*D*	1.257	0.215	0.171	8.81×10^{-2}	0.119
	$\delta_{h2} = 20$ m, $\delta_{v2} = 4$ m	10,000 LHS	–	1.253	0.190	0.152	7.87×10^{-2}	
3	$\delta_{h1} = 40$ m, $\delta_{v1} = 4$ m	MARS–MCS (this study)	20*D*	1.260	0.181	0.144	6.89×10^{-2}	0.170
	$\delta_{h2} = 40$ m, $\delta_{v2} = 2$ m	10,000 LHS	–	1.261	0.181	0.143	5.89×10^{-2}	
4	$\delta_{h1} = 20$ m, $\delta_{v1} = 4$ m	MARS–MCS (this study)	15*D*	1.255	0.187	0.149	7.88×10^{-2}	0.108
	$\delta_{h2} = 40$ m, $\delta_{v2} = 4$ m	10,000 LHS	–	1.255	0.180	0.143	7.11×10^{-2}	
5	$\delta_{h1} = 40$ m, $\delta_{v1} = 2$ m	MARS–MCS (this study)	20*D*	1.242	0.164	0.132	6.46×10^{-2}	0.023
	$\delta_{h2} = 40$ m, $\delta_{v2} = 4$ m	10,000 LHS	–	1.239	0.162	0.131	6.31×10^{-2}	

Note: The symbol "–" means not applicable.

approximately similar. All these results confirm that the proposed approach can efficiently evaluate the reliability of heterogeneous slopes with sufficient accuracy while considering multiscale spatial variability of soil properties.

6.3. Influence of multiscale spatial variability of soil properties

As mentioned above, soil properties will exhibit multiscale spatial variability in multi-layered soils. However, few efforts have been made to quantify the influence of this kind of spatial soil variability on slope reliability. Thus, this section intends to address this problem involved in the aforementioned heterogeneous slope using the proposed approach where the accuracy has been validated above. To show the multiscale spatial variability of the undrained strength of this slope, Fig. 11 schematically plots the random fields of s_{u1} and s_{u2} for the five cases in Table 4 based on a typical simulation. It is worth noting that in Fig. 11a, the undrained strengths s_{u1} and s_{u2} vary in an identical level (i.e.,

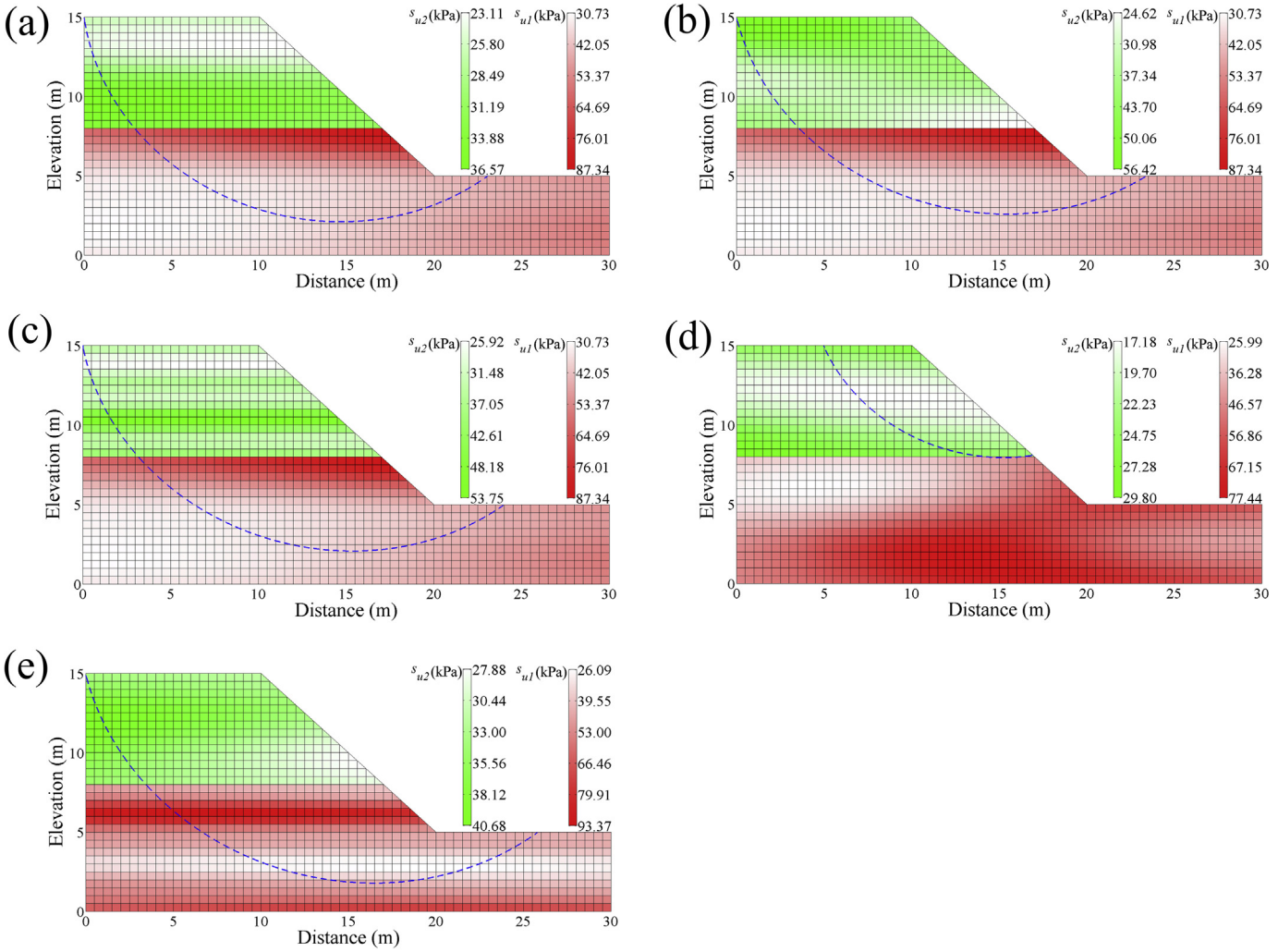

Figure 11. Typical random field realizations for the five cases in Table 4. (a) Case No. 1, FS = 1.183; (b) Case No. 2, FS = 1.261; (c) Case No. 3, FS = 1.234; (d) Case No. 4, FS = 1.018; (e) Case No. 5, FS = 1.227. Interpretation of the references to color in this figure can be referred to the web version of this article.

$\delta_{h1} = \delta_{h2} = 40$ m and $\delta_{v1} = \delta_{v2} = 4$ m) in their respective spatial domains, indicating that no multiscale spatial soil variability is considered. This is also the common way for characterizing the spatial soil variability in layered soils in the literature (e.g., Huang, 2010; Li et al., 2015; Jiang and Huang, 2016; Li et al., 2016a). Hence, this case (i.e., case No. 1) is considered for comparison purpose to explicitly illustrate the influence of the multiscale spatial variability of soils. Compared with Fig. 11a, b and c presents more rapid fluctuations in clay 2 because smaller horizontal and vertical SOFs (i.e., $\delta_{h2} = 20$ m in Fig. 11b and $\delta_{v2} = 2$ m in Fig. 11c) are adopted in the two figures, respectively, while the other SOFs are remained the same as those in Fig. 11a. Similarly, Fig. 11d and e also presents obvious multiscale spatial variability due to the influence of clay 1. These observations are consistent with what has been presented by Huang (2010), who however has not further consider such multiscale spatial variability in his work. The limitation of Huang (2010) will be tackled properly in the present study.

Fig. 12a and b shows the variation of P_f with respect to various horizontal and vertical SOFs, respectively, and both of the two subfigures concern the influence of three scenarios. Scenario 1 considers that the undrained strengths s_{u1} and s_{u2} share the same level of spatial variability in their respective domains, and it is marked by the pink line with squares. Scenario 2 denotes the situation where only a horizontal or vertical SOF of s_{u1} in clay 1 changes but the other SOFs, including those associated with s_{u2} in clay 2 and another SOF in clay 1, remain the same as those in the baseline case (i.e., $\delta_{h1} = \delta_{h2} = 40$ m and $\delta_{v1} = \delta_{v2} = 4$ m), which is marked by the red line with circles. In contrast to scenario 2, scenario 3 which is characterized by the blue line with triangles in Fig. 12 only involves the change of a horizontal or vertical SOF of s_{u2} in clay 2, whereas the other SOFs are kept the same as those in the baseline case. Herein, it is worth noting that scenario 1 does not take the multiscale spatial variability of soil properties into account, while scenarios 2 and 3 do consider, aiming at highlighting the influence of the spatial variability in clays 1 and 2, respectively.

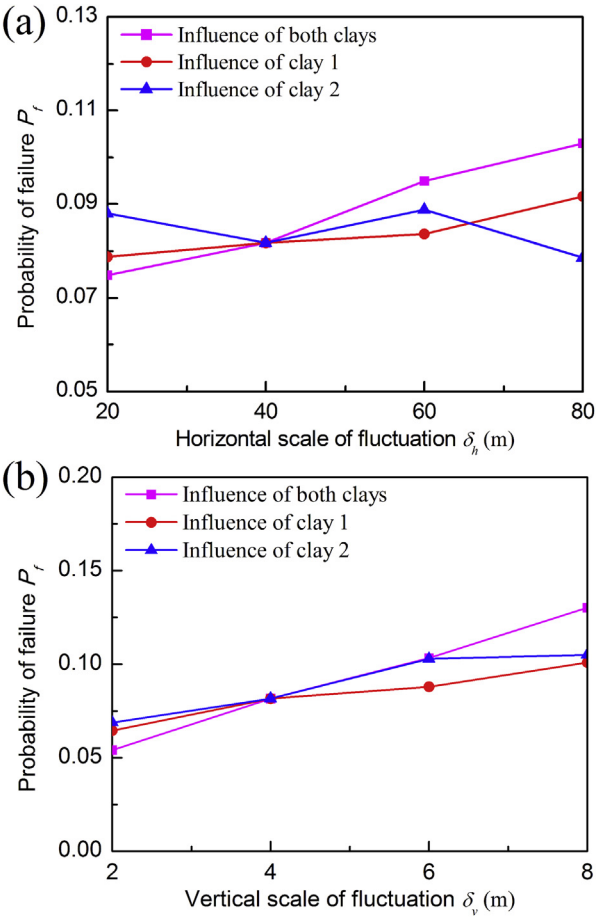

Figure 12. Influence of SOFs in different clays on P_f of the heterogeneous slope. (a) Horizontal scale of fluctuation; (b) vertical scale of fluctuation.

According to Fig. 12a, the values of P_f obtained for scenario 1 increase with the increase of δ_h, which agrees well with many other published results (e.g., Li et al., 2015) that are also evaluated by neglecting the multiscale spatial variability of soil properties. The results associated with scenario 2 also present an increasing trend that is similar to scenario 1 but varies more slightly, whereas the results associated with scenario 3 fluctuate around 8.00×10^{-2}. Generally, there are differences among the results underlying all three scenarios. Compared with the values of P_f for scenario 1, the results obtained for both scenarios 2 and 3 are overestimated and underestimated when δ_h is smaller and larger than 40 m, respectively. The reason mainly lies in the fact that the δ_h in both scenarios 2 and 3 becomes relatively larger and smaller than the δ_h in scenario 1 when δ_h is smaller and larger than 40 m, respectively. This will increases and decreases the probability that the undrained strength has weak values, which finally induces higher and lower values of P_f, when δ_h is smaller and larger than 40 m, respectively. However, the difference of the aforementioned overestimation or underestimation is not major. Additionally, compared with the results associated with scenario 2, the δ_h in caly 2 (i.e., scenario 3) seems to have less influence on the P_f.

On the other hand, in Fig. 12b, the P_f values increase with the δ_v for all the three scenarios which is as expected. It is also observed from the figure that similar to Fig. 12a, the results based on scenario 1 are underestimated and overestimated when δ_v is smaller and larger than 4 m, respectively. The underlying reasons are very similar to those for Fig. 12a and are not repeated herein. Overall, comparing Fig. 12a and b, it is found that δ_v generally affects the P_f more significantly than δ_h, which is in good consistence with the results as reported in the literature (e.g., Cho, 2010; Ji and Low, 2012; Li et al., 2015). Furthermore, it is of practical significance to consider the multiscale spatial variability of soil properties in reliability analysis of heterogeneous slopes, especially for those highly related to cost-effective and accurate designs, although conventional uniform spatial variability assumption would not produce much difference.

7. Summary and conclusions

This paper proposed an efficient MARS–MCS method for the reliability analysis of slopes in spatially variable soils. The proposed approach is illustrated by two slope examples that are characterized with different spatial variabilities. Accordingly, the influence of multiscale spatial variability of soil properties on slope reliability is explored. The following conclusions can be drawn from this study:

(1) The relationship between FS and soil strength parameters of slopes in spatially variable soils can be well established using MARS with the aid of K–L expansion. The widely used empirical guideline for selecting the training sample size is applicable to the calibration of the MARS model in this study. K–L expansion can discretize the random fields of soil strength parameters by using few random variables, which contribute significantly to the accuracy and efficiency of the MARS model. Moreover, K–L expansion can be easily extended to simulate globally non-stationary non-Gaussian random fields.

(2) The proposed MARS–MCS approach can efficiently estimate the P_f of slopes in spatially variable soils with sufficient accuracy. This approach is also relatively robust to the influence of

different statistics (e.g., COVs and SOFs) of soil properties, thereby suggesting its effectiveness for slope stability with both high and low levels of failure probability. Thus, this approach provides an effective and practical tool for addressing slope reliability problems that concern time-consuming deterministic stability models with low failure probability levels.

(3) Neglecting the multiscale spatial variability of soil properties can overestimate or underestimate the probability of slope failure, depending on the difference between the actual SOF in a particular soil layer and the assumed SOF for all layers. However, the difference in such overestimation or underestimation is small. Nevertheless, the multiscale spatial variability of soil properties must still be considered in the reliability analysis of heterogeneous slopes, especially for those highly related to cost effective and accurate designs.

(4) The difference between the undrained strengths in different layers is insignificant. Thus, future studies on reliability analysis should be conducted on slopes involving weak layers to further explore the influence of multiscale spatial variability of soil properties on the probability of slope failure.

Acknowledgements

The work presented in this paper was supported by The Hong Kong Polytechnic University through the project RU3Y and the Research Grant Council through the project PolyU 5128/13E, National Natural Science Foundation of China (Grant No. 51778313) and Cooperative Innovation Center of Engineering Construction and Safety in Shangdong Blue Economic Zone. These financial supports are gratefully acknowledged.

References

Cheng, M.Y., Cao, M.T., 2014. Accurately predicting building energy performance using evolutionary multivariate adaptive regression splines. Applied Soft Computing 22, 178–188.

Ching, J., Phoon, K.K., 2013. Effect of element sizes in random field finite element simulations of soil shear strength. Computers and Structures 126, 120–134.

Ching, J., Wang, J.S., 2016. Application of the transitional Markov chain Monte Carlo algorithm to probabilistic site characterization. Engineering Geology 203, 151–167.

Cho, S.E., 2010. Probabilistic assessment of slope stability that considers the spatial variability of soil properties. Journal of Geotechnical and Geoenvironmental Engineering 136 (7), 975–984.

Cho, S.E., 2012. Probabilistic analysis of seepage that considers the spatial variability of permeability for an embankment on soil foundation. Engineering Geology 133–134, 30–39.

Dasaka, S.M., Zhang, L.M., 2012. Spatial variability of in situ weathered soil. Géotechnique 62 (5), 375–384.

Fenton, G.A., Vanmarcke, E.H., 1990. Simulation of random fields via local average subdivision. Journal of Engineering Mechanics 116 (8), 1733–1749.

Fenton, G.A., Griffiths, D.V., 2003. Bearing-capacity prediction of spatially random c–φ soils. Canadian Geotechnical Journal 40 (1), 54–65.

Friedman, J.H., 1991. Multivariate adaptive regression splines. The Annals of Statistics 19 (1), 1–67.

Griffiths, D.V., Fenton, G.A., 2004. Probabilistic slope stability analysis by finite elements. Journal of Geotechnical and Geoenvironmental Engineering 130 (5), 507–518.

Griffiths, D.V., Huang, J., Fenton, G.A., 2011. Probabilistic infinite slope analysis. Computers and Geotechnics 38 (4), 577–584.

Hastie, T., Tibshirani, R., Friedman, J.H., 2009. The Elements of Statistical Learning: Data Mining, Inference and Prediction, second ed. Springer, California. 745 pp.

Huang, J., 2010. System reliability of slopes by RFEM. Soils and Foundations 50 (3), 343–353.

Huang, J., Lyamin, A.V., Griffiths, D.V., Krabbenhoft, K., Sloan, S.W., 2013. Quantitative risk assessment of landslide by limit analysis and random fields. Computers and Geotechnics 53, 60–67.

Huang, S.P., Quek, S.T., Phoon, K.K., 2001. Convergence study of the truncated Karhunen–Loeve expansion for simulation of stochastic processes. International Journal for Numerical Methods in Engineering 52 (9), 1029–1043.

Ji, J., Liao, H.J., Low, B.K., 2012. Modeling 2-D spatial variation in slope reliability analysis using interpolated autocorrelations. Computers and Geotechnics 40, 135–146.

Ji, J., Low, B.K., 2012. Stratified response surfaces for system probabilistic evaluation of slopes. Journal of Geotechnical and Geoenvironmental Engineering 138 (11), 1398–1406.

Ji, J., 2014. A simplified approach for modeling spatial variability of undrained shear strength in out-plane failure mode of earth embankment. Engineering Geology 183, 315–323.

Ji, J., Zhang, C., Gao, Y., Kodikara, J., 2018. Effect of 2D spatial variability on slope reliability: a simplified FORM analysis. Geoscience Frontiers 9 (6), 1631–1638. https://doi.org/10.1016/j.gsf.2017.08.004.

Ji, J., Zhang, C., Gui, Y., Lü, Q., Kodikara, J., 2017. New observations on the application of LS-SVM in slope system reliability analysis. Journal of Computing in Civil Engineering 31 (2), 06016002.

Jiang, S.H., 2014. A Non-intrusive Stochastic Method for Slope Reliability in Hydroelectricity Engineering. Ph.D thesis. Wuhan University, 224 pp.

Jiang, S.H., Li, D.Q., Zhang, L.M., Zhou, C.B., 2014. Slope reliability analysis considering spatially variable shear strength parameters using a non-intrusive stochastic finite element method. Engineering Geology 168, 120–128.

Jiang, S.H., Li, D.Q., Cao, Z.J., Zhou, C.B., Phoon, K.K., 2015. Efficient system reliability analysis of slope stability in spatially variable soils using Monte Carlo simulation. Journal of Geotechnical and Geoenvironmental Engineering 141 (2), 04014096.

Jiang, S.H., Huang, J.S., 2016. Efficient slope reliability analysis at low-probability levels in spatially variable soils. Computers and Geotechnics 75, 18–27.

Kang, F., Han, S., Salgado, R., Li, J., 2015. System probabilistic stability analysis of soil slopes using Gaussian process regression with Latin hypercube sampling. Computers and Geotechnics 63, 13–25.

Laloy, E., Rogiers, B., Vrugt, J.A., Mallants, D., Jacques, D., 2013. Efficient posterior exploration of a high-dimensional groundwater model from two-stage Markov chain Monte Carlo simulation and polynomial chaos expansion. Water Resources Research 49 (5), 2664–2682.

Li, D., Chen, Y., Lu, W., Zhou, C., 2011. Stochastic response surface method for reliability analysis of rock slopes involving correlated non-normal variables. Computers and Geotechnics 38 (1), 58–68.

Li, D.Q., Jiang, S.H., Cao, Z.J., Zhou, W., Zhou, C.B., Zhang, L.M., 2015. A multiple response-surface method for slope reliability analysis considering spatial variability of soil properties. Engineering Geology 187, 60–72.

Li, D.Q., Xiao, T., Cao, Z.J., Zhou, C.B., Zhang, L.M., 2016a. Enhancement of random finite element method in reliability analysis and risk assessment of soil slopes using Subset Simulation. Landslides 13, 293–303.

Li, K.S., Lumb, P., 1987. Probabilistic design of slopes. Canadian Geotechnical Journal 24 (4), 520–535.

Li, X.Y., Zhang, L.M., Gao, L., Zhu, H., 2017. Simplified slope reliability analysis considering spatial soil variability. Engineering Geology 216, 90–97.

Liu, L.L., Cheng, Y.M., 2016. Efficient system reliability analysis of soil slopes using multivariate adaptive regression splines-based Monte Carlo simulation. Computers and Geotechnics 79, 41–54.

Liu, L.L., Cheng, Y.M., Jiang, S.H., Zhang, S.H., Wang, X.M., Wu, Z.H., 2017a. Effects of spatial autocorrelation structure of permeability on seepage through an embankment on a soil foundation. Computers and Geotechnics 87, 62–75.

Liu, L.L., Cheng, Y.M., Zhang, S.H., 2017b. Conditional random field reliability analysis of a cohesion-frictional slope. Computers and Geotechnics 82, 173–186.

Low, B.K., 2007. Reliability analysis of rock slopes involving correlated nonnormals. International Journal of Rock Mechanics and Mining Sciences 44 (6), 922–935.

Low, B.K., 2014. FORM, SORM, and spatial modeling in geotechnical engineering. Structural Safety 49, 56–64.

Lu, Z.M., Zhang, D.X., 2007. Stochastic simulations for flow in nonstationary randomly heterogeneous porous media using a KL-based moment-equation approach. Multiscale Modeling & Simulation 6 (1), 228–245.

Phoon, K.K., Kulhawy, F.H., 1999. Characterization of geotechnical variability. Canadian Geotechnical Journal 36, 612–624.

Phoon, K.K., Huang, S.P., Quek, S.T., 2002. Implementation of Karhunen–Loeve expansion for simulation using a wavelet-Galerkin scheme. Probabilistic Engineering Mechanics 17 (3), 293–303.

Santoso, A.M., Phoon, K.K., Quek, S.T., 2011. Effects of soil spatial variability on rainfall-induced landslides. Computers and Structures 89, 893–900.

Silvestrini, R.T., Montgomery, D.C., Jones, B., 2013. Comparing computer experiments for the Gaussian process model using integrated prediction variance. Quality Engineering 25 (2), 164–174.

Srivastava, A., Sivakumar Babu, G.L., Haldar, S., 2010. Influence of spatial variability of permeability property on steady state seepage flow and slope stability analysis. Engineering Geology 110, 93–101.

Sudret, B., Kiureghian, A.D., 2002. Comparison of finite element reliability methods. Probabilistic Engineering Mechanics 17 (4), 337–348.

Wang, Y., Cao, Z.J., Au, S.K., 2011. Practical reliability analysis of slope stability by advanced Monte Carlo simulations in a spreadsheet. Canadian Geotechnical Journal 48, 162–172.

Wang, Y., Cao, Z., Li, D., 2016. Bayesian perspective on geotechnical variability and site characterization. Engineering Geology 203, 117–125.

Zhang, W.G., Goh, A.T.C., 2013. Multivariate adaptive regression splines for analysis of geotechnical engineering systems. Computers and Geotechnics 48, 82–95.